Am J Cancer Res 2026;16(6):2493-2502
www.ajcr.us /ISSN:2156-6976/ajcr0170950

Original Article

Serum amyloid P component suppresses melanoma growth and metastasis by inhibiting CCL1 secretion from macrophages

Pei Tang[1*], Ying Wang[1*], Bo Zhao[2], Bohan Zheng[1], Bin Li[1], Shuang Wu[1], Xiaoming Li[1], Lijing Wang[1], Cuiling Qi[1]

[1]Laboratory of Oncology and Immunology, School of Basic Medical Sciences, Guangdong Pharmaceutical University, Guangzhou 510006, Guangdong, China; [2]Department of Rehabilitation, The First Affiliated Hospital, Jinan University, Guangzhou 510632, Guangdong, China. [*]Equal contributors.

Received December 22, 2025; Accepted June 1, 2026; Epub June 15, 2026; Published June 30, 2026

Abstract: The incidence of melanoma, which is among the most common skin cancers, has significantly increased at an alarming rate over the past decade. Serum amyloid P component (SAP), a member of the pentraxin (PTX) family, is a major acute-phase protein in mice. The effects of SAP on melanoma and the mechanisms underlying these effects remain unclear. In the current study, we established xenograft and metastatic melanoma models in SAP-overexpressing (SAP-Tg) mice to determine the effect of SAP on the progression of melanoma. Compared with wild-type (WT) mice, SAP-Tg mice developed tumors with smaller volumes and fewer metastatic foci, and the degree of cell proliferation within the transplanted tumors was significantly decreased by SAP. Further study indicated that SAP inhibited melanoma growth and metastasis by suppressing CC-chemokine 1 (CCL1) secretion from activated macrophages, while CCL1 promoted the migration and invasion of B16F10 melanoma cells. Furthermore, SAP-induced CCL1 downregulation suppressed Ras/p-ERK pathway activation. These findings indicate a new effect of SAP mediated via a novel mechanism and provide direct evidence that SAP may have therapeutic value for melanoma.

Keywords: SAP, melanoma, CCL1, melanoma growth, melanoma metastasis, macrophage

Introduction

Serum amyloid P component (SAP) is a member of the pentraxin (PTX) protein family [1], which contains two subfamilies: short-chain PTXs, including SAP and C-reactive protein (CRP), and long-chain PTXs, such as PTX3 [2]. SAP and CRP are acute-phase reactive proteins. However, unlike CRP, which is an acute-phase protein in humans, SAP is a major acute-phase protein in mice [3]. SAP is produced mainly in the liver through stimulation by TNF-alpha and interleukin-6. Merchant S et al. demonstrated that photodynamic therapy (PDT)-treated tumor cells can directly produce SAP [4]. Additionally, SAP can inhibit hepatic and cardiac fibrosis [5-8], dermal wound healing [9], allergic airway disease [10], radiation-induced oral mucositis [11], autoimmune disease [12], kidney injury [13] and so forth. Furthermore, recombinant human SAP enhanced the pulmonary function of pulmonary fibrosis patients in a phase 1B clinical trial [14]. Levo Y et al. demonstrated that the serum concentration of SAP in patients with breast cancer was significantly increased and correlated with breast cancer progression [3]. Moreover, SAP levels were not found to be altered in patients with colon cancer [3]. While the role of SAP in breast cancer has been explored, research on the role of SAP in melanoma remains extremely limited and fragmented. A recent study revealed that a SAP-derived microprotein can modulate chaperone-mediated autophagy (CMA) to promote PD-L1 degradation in melanoma, suggesting the potential of SAP as a therapeutic tool [15]. However, whether SAP plays a role in melanoma is not yet known.

Melanoma is among the most common skin cancers, and its incidence has significantly increased at an alarming rate over the past

https://doi.org/10.62347/YYHY2072

decade [16-18]. Additionally, melanoma is among the most aggressive and deadly forms of skin cancer. Once melanoma enters the metastatic stage, it has a poor prognosis; the five-year survival of patients with metastatic melanoma is less than 5%, with a median survival period of approximately 8.5 months [19]. Currently, BRAF and MEK are the most common targets for the clinical treatment of melanoma [20]. Nevertheless, long-term targeted treatment frequently induces drug resistance, tumor recurrence and distant metastasis, thus limiting clinical therapeutic efficacy [21]. In recent years, the remodeling of the melanoma tumor microenvironment, especially macrophage infiltration and macrophage-derived chemokine regulatory networks, has become hot research topic because the tumor microenvironment profoundly affects melanoma proliferation, invasion and metastasis. However, crosstalk between upstream molecules and macrophage chemokine pathways remains poorly understood [22]. Therefore, research into the mechanisms responsible for melanoma is necessary to identify new strategies for treating this disease.

Chemokines play important roles in the progression of malignant tumors [23-25]. CC-chemokine 1 (CCL1), which is secreted by activated macrophages, T cells, mast cells, and endothelial cells, can promote the migration of melanoma cells to the lymph nodes through CCR8, the receptor for CCL1 [26]. CCL1 has also been shown to activate the Ras/MAP-kinase pathway in BW5147 thymic lymphoma cells [26]. However, the role of the CCL1/Ras/MAP kinase pathway in melanoma progression and the relationship between SAP and the CCL1/Ras/MAP kinase pathway remain unknown.

In the current study, we showed that tumor volume and weight were smaller in SAP-Tg mice than in WT mice, and SAP-Tg mice developed fewer metastatic tumors on pulmonary and liver surfaces. We also revealed that SAP suppressed the secretion of CCL1 by activated macrophages. In addition, we showed that CCL1 promoted the migration and invasion of B16F10 melanoma cells and activated the Ras/MAPK pathway. Furthermore, the expression of Ras and p-Erk1/2 in tumor tissues was significantly lower in SAP-Tg mice than in WT mice. Taken together, these results show that SAP inhibits the growth and metastasis of melanoma through the CCL1/Ras/MAPK pathway.

Materials and methods

Mice

SAP-overexpressing (SAP-Tg) mice and SAP-knockout (SAP KO) mice were obtained from Professor Geng, and the mouse phenotypes were detected by PCR using the following primers: SAP-Tg mice, 5'-TACAGTGACCTTTCCCGCTCT CAGAGTCT-3' (forward) and 5'-ACGACTCACTA-TAGG GCGAATTGGGTACA C-3' (reverse); and SAP KO mice, 5'-TACAGTGACCTTTCCCGCTCTC-AGA GTCT-3' (forward) and 5'-ACGACTCACTAT-AGGGCGAATTGGGTACAC-3' (reverse). Animal housing and experimental procedures followed institutional guidelines.

Transplanted tumor growth assay and survival curves

All animal experiments were carried out on 6- to 8-week-old female WT mice, female SAP-Tg mice and SAP KO mice. The mouse melanoma cell line B16F10 (B16) was passaged in RPMI-1640 medium supplemented with 10% FCS. A total of 1×10^5 cells suspended in 200 μL of phosphate-buffered saline (PBS) were injected subcutaneously into the right armpits of the mice. The length and width of the tumors were measured with a Vernier caliper, and the tumor volume was calculated as $0.52 \times \text{length} \times \text{width}^2$. When the largest tumor mass exceeded 2 cm^3, euthanasia was performed according to institutional guidelines, and the tumors were weighed. For the survival assay, the mice were kept in a pathogen-free environment and euthanized by cervical dislocation when their general condition severely declined. The time was recorded. All animal experiments were approved by the Medical Research Animal Ethics Committee of Guangdong Pharmaceutical University and were conducted in accordance with relevant national and international guidelines (Approval No. gdpulacspf2021005).

Experimental metastasis assay

For the experimental metastasis model, 1×10^5 B16F10 cells in 200 μL of PBS were injected intravenously into the tail vein. The mice were sacrificed after 3 weeks, after which their

lungs, livers, kidneys, brains and mesentery were carefully checked. The surface metastatic colonies were counted under a stereomicroscope.

Evaluation of tumor metastasis

The lungs, livers, kidneys and brains of WT and SAP-Tg mice were embedded in paraffin, serially sectioned and stained with hematoxylin-eosin (H&E). Next, two experienced pathologists who were blinded to the source of the tissues viewed the H&E-stained slides and determined the number of metastatic and micrometastatic foci. The number of metastatic foci in every mouse was determined by the following equation: number of metastatic foci = number of foci in all the sections in every mouse/number of sections.

Immunohistochemical staining

Immunohistochemical staining was performed to determine whether the overexpression of SAP affects the proliferation of tumor cells. Before immunohistochemical staining was performed, 100 mg/kg 5-bromo-2'-deoxyuridine (BrdU; cat. no. B5002; Sigma) was intraperitoneally injected into B16 xenograft mice. After 1 h, the mice were sacrificed. Briefly, 3 μm sections were dewaxed, hydrated and incubated in a 3% H_2O_2-methanol solution at 37°C for 30 min. After being blocked with 10% BSA, the sections were incubated with an anti-BrdU (1:100 dilution; cat. No. sc-32323; Santa Cruz, CA, USA) primary antibody overnight at 4°C. The next day, the sections were detected using an HRP-conjugated secondary antibody and stained with dimethylaminoazobenzene (DAB). After the sections were counterstained with hematoxylin, the number of $BrdU^+$ cells was counted in a random 400× field as a percentage of the total number of cells per field.

CHiP protein assay and Enzyme-linked immunosorbent assay (ELISA)

Mouse protein CHiP assay kits were purchased from RayBiotech (cat. No. AAM-INF-1; RayBiotech, Guangzhou, China). The Mouse Inflammatory Array Kit contained 43 different inflammatory factors. The CHiP protein assay was performed according to the manufacturer's instructions. Briefly, serum was obtained from WT and SAP-Tg mice into which melanoma cells had been transplanted. The diluted serum was incubated with the antibody arrays overnight at 4°C. The arrays were subsequently washed to remove unbound protein prior to incubation with a biotinylated antibody cocktail. The membranes were subsequently washed and incubated with horseradish peroxidase-streptavidin. The arrays were quantified by densitometry using the RayBiotech Q-analyser Tool (RayBiotech).

CCL1 concentrations in serum, tissue homogenates and cell culture supernatants were measured using commercial ELISA kits (JNOLNBIO, Shanghai, China) according to the manufacturer's instructions.

Wound-healing assay

B16F10 cells were cultured in a 24-well plate at a density of 5×10^5 cells/well in 500 μL of RPMI-1640 medium supplemented with 10% FBS. After 18 h, the B16F10 cell monolayer was scratched with a 200 μL pipette tip at a 90° angle to create a wound. The cells were subsequently washed twice with PBS and incubated in fresh medium (10% FBS) supplemented with PBS or CCL1 (12.5 ng/mL, 25 ng/mL or 50 ng/mL). Images were taken at 0 h and 18 h under an inverted microscope (4× objective). Migration was quantified by measuring the diameter of the wound as the average diameter from three different locations.

Cell migration and invasion assays

Cell migration and invasion assays were performed as previously described using a Boyden chamber containing a polycarbonate filter (Transwell 24, 8-mm pore; Costar, Cambridge, MA, USA). B16F10 cells were resuspended in serum-free medium and then added to the chamber coated with (cell invasion assay) or without (cell migration assay) Matrigel (cat. No. 356234; BD Biosciences San Jose, CA, USA) at a density of 5×10^5. PBS, CCL1 (12.5 ng/mL, 25 ng/mL or 50 ng/mL) or CCL1 (50 ng/mL) supplemented with R243 (1 μM) was added to the upper chamber. After being allowed to migrate or invade for 24 h, the cells that remained in the chamber were removed with a cotton swab. The cells that had migrated or invaded the lower surface of the chamber were fixed with 4% paraformaldehyde and then stained with 1% crystal violet. The numbers of

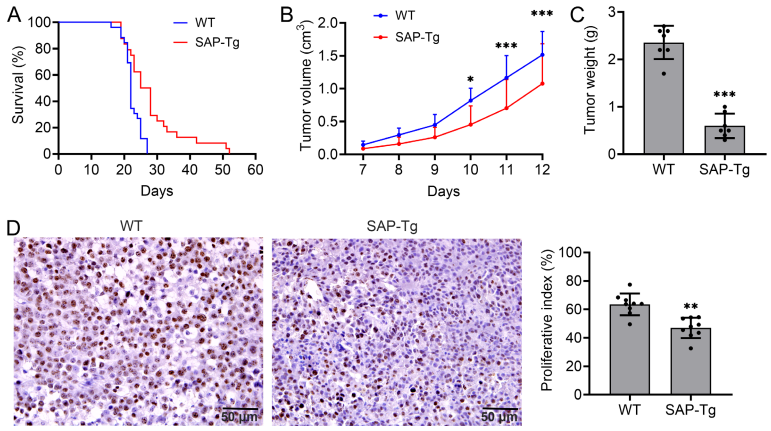

Figure 1. SAP inhibits melanoma growth. A. Survival curve of mice with subcutaneous tumors. The decrease in survival was statistically significant at 30 days, when institutional animal welfare guidelines required termination of the experiment. B. The length and width of tumors from mice subcutaneously injected with B16F10 cells were measured, and tumor volume was calculated. The average tumor volume of the mice in each group was plotted against time. C. The weight of the primary tumors on Day 12. D. Immunohistological staining of Ki67 demonstrated that tumor cell proliferation was significantly decreased in the SAP-Tg mice. Scale bars, 50 μm (magnification: 400×). The results are representative of at least four sections per mouse from a minimum of three mice per group. Data are presented as the means ± SD. **P < 0.05*; ***P < 0.01*; ****P < 0.001*.

migrating or invading cells were determined by counting the cells in five randomly selected fields in the center of the filter under a phase-contrast microscope. The experiments were performed in triplicate.

Western blotting

Transplanted tumor tissues from WT and SAP-Tg mice were harvested for protein extraction. Equal amounts of total protein were then separated by SDS-PAGE (10% polyacrylamide gel) and transferred onto nitrocellulose membranes. The membranes were probed with primary antibodies against Ras, p-ERK and ERK (Cell Signaling Technology, Danvers, MA, USA), followed by incubation with horseradish peroxidase-conjugated secondary antibodies. Western blotting was performed with a chemiluminescence (ECL) kit (GE Healthcare, Pittsburgh, PA, USA) according to the manufacturer's instructions. The band intensities were quantified by densitometry using ImageJ software.

Statistical analysis

Data analysis was performed using GraphPad software (GraphPad Prism v10.6; GraphPad Software, CA). Quantitative data are presented as the mean ± standard deviation (SD). Statistical significance was determined with a two-tailed Student's t test for two-group comparisons or one-way ANOVA followed by Bonferroni post hoc correction for multiple-group comparisons. For multiple-group comparisons with time-dependent variables, two-way repeated-measures ANOVA was performed. For all the tests, $P < 0.05$ or < 0.01 was considered to indicate statistical significance.

Results

SAP suppresses melanoma growth

To investigate the potential role of SAP in tumor growth, B16F10 melanoma cells were injected subcutaneously into SAP-Tg and WT mice, after which the tumor volume was evaluated from Days 7 to 12. In all the mice, the inoculated B16F10 melanoma cells formed solid, round tumors with well-defined margins in the right armpit. Furthermore, the tumor volume and weight at 7-12 days of age were smaller for SAP-Tg mice than for WT mice examined (**Figure 1B**, **1C**). The time of death of each mouse was also related to the volume and weight of the primary tumor, and survival significantly differed between the WT and SAP-Tg mice (**Figure 1A**) up to the time point at which the tumors reached the size required to terminate the experiment. In addition, we investigated whether SAP was involved in the proliferation of tumor cells and found a significant reduction in the proliferation of tumor cells from SAP-Tg mice (**Figure 1D**). We also detected the effect of SAP on melanoma growth in SAP KO mice and found that the melanoma volume was greater in SAP KO mice than in WT mice between 7 and 12 days of age (Figure S1A). These results demonstrate that SAP significantly inhibits melanoma growth.

SAP inhibits lung and liver metastasis

Given that SAP inhibits melanoma growth, we wanted to determine whether SAP affects mel-

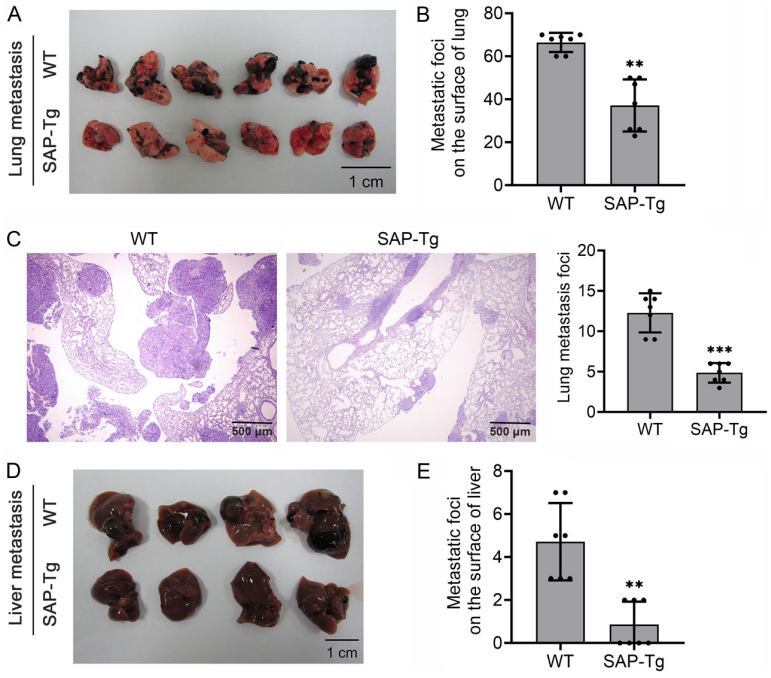

Figure 2. SAP overexpression suppresses lung and liver metastasis of B16F10 cells. (A) Gross images of melanoma lung metastasis in WT and SAP-Tg mice. (B) The statistical analysis revealed fewer metastatic foci on the lung surface in SAP-Tg mice than in WT mice. (C) H&E staining of the lungs of SAP-Tg mice, which developed fewer micrometastatic foci than those of WT mice did. (D) Gross images of melanoma liver metastasis in WT and SAP-Tg mice. (E) The statistical analysis revealed fewer metastatic foci on the liver surface in SAP-Tg mice than in WT mice. Scale bars, 1 cm in (A, D); 500 μm (magnification: 40×) in (C). Data are presented as the means ± SD. ***P < 0.01*; ****P < 0.001*.

anoma metastasis. To determine the role of SAP in melanoma metastasis, B16F10 melanoma cells were injected via the tail vein into WT and SAP-Tg mice. Metastatic colonies formed in the lungs and livers of WT and SAP-Tg mice following the injection of B16F10 melanoma cells and were observed as black spots. At 21 days after injection, the SAP-Tg mice developed fewer metastatic tumors on their pulmonary and liver surfaces (**Figure 2A**, **2B**, **2D**, **2E**). H&E staining of the lung revealed the homology of the B16F10 cells. The H&E staining image with higher magnification shows the morphology of tumor cells (Figure S2). The metastatic and micrometastatic foci were quantified under low-power magnification, which indicated similar results (**Figure 2C**). In addition, no metastatic foci were observed in the brains or kidneys of either wild-type or SAP-Tg mice. To confirm the effect of SAP on melanoma metastasis, we established a metastasis model using SAP KO mice. Compared with WT mice, SAP KO mice developed more metastatic foci on the surface of the lung (Figure S1B and S1C). These results demonstrate that SAP significantly suppresses melanoma metastasis.

SAP decreases the concentration of CCL1 secreted by macrophages

To determine how SAP inhibits melanoma growth and metastasis, a protein CHiP array analysis was performed to detect changes in the levels of inflammation-related proteins in the serum of SAP-Tg mice and WT mice with melanoma. Serum CCL1 levels were decreased in the melanoma-bearing SAP-Tg mice compared with the melanoma-bearing WT mice (**Figure 3A**). We also found that the concentrations of CCL1 in the serum of tumor-bearing SAP-Tg mice and in melanoma homogenates from SAP-Tg mice were lower than those in the serum of and melanoma homogenates from WT mice (**Figure 3B**). However, the serum CCL1 concentration in the normal mice was not affected (**Figure 3B**). In addition, in the melanoma metastasis model, the concentration of CCL1 in serum and melanoma homogenates from SAP-Tg mice was lower than that in serum and melanoma homogenates from WT mice (**Figure 3C**). Then, we cultured the RAW264.7 macrophage line with the SAP protein, and the ELISA results revealed that SAP significantly decreased the secretion of CCL1 by RAW264.7 cells compared with PBS-treated control cells (**Figure 3D**). We also cultured macrophages derived from WT and SAP-Tg mice and found that the secretion of CCL1 was lower in the macrophage culture medium derived from SAP-Tg mice than in that derived from WT mice (**Figure 3E**). These results show that SAP inhibits the secretion of CCL1 by macrophages.

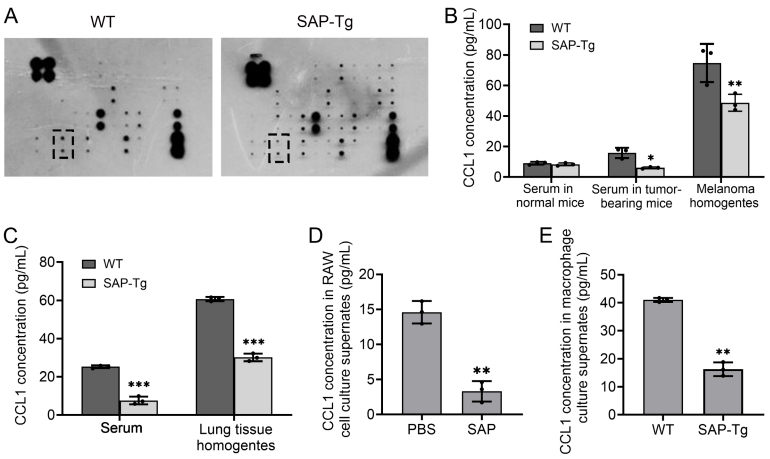

Figure 3. SAP decreases the concentration of CCL1 secreted by macrophages. A. The protein CHiP array data revealed that the serum level of CCL1 was lower in the melanoma-bearing SAP-Tg mice than in melanoma-bearing WT mice. B. Serum and melanoma homogenate levels of CCL1 in normal and tumor-bearing WT and SAP-Tg mice. C. Serum and melanoma homogenate levels of CCL1 in melanoma lung metastases from WT and SAP-Tg mice. D. Compared with the control treatment, treatment with 50 ng/mL SAP for 24 h significantly decreased the level of CCL1 in RAW264.7 cell culture medium. E. The CCL1 concentration in the culture medium of macrophages derived from WT and SAP-Tg mice. Data are presented as the means ± SD. *$P < 0.05$; **$P < 0.01$; ***$P < 0.001$.

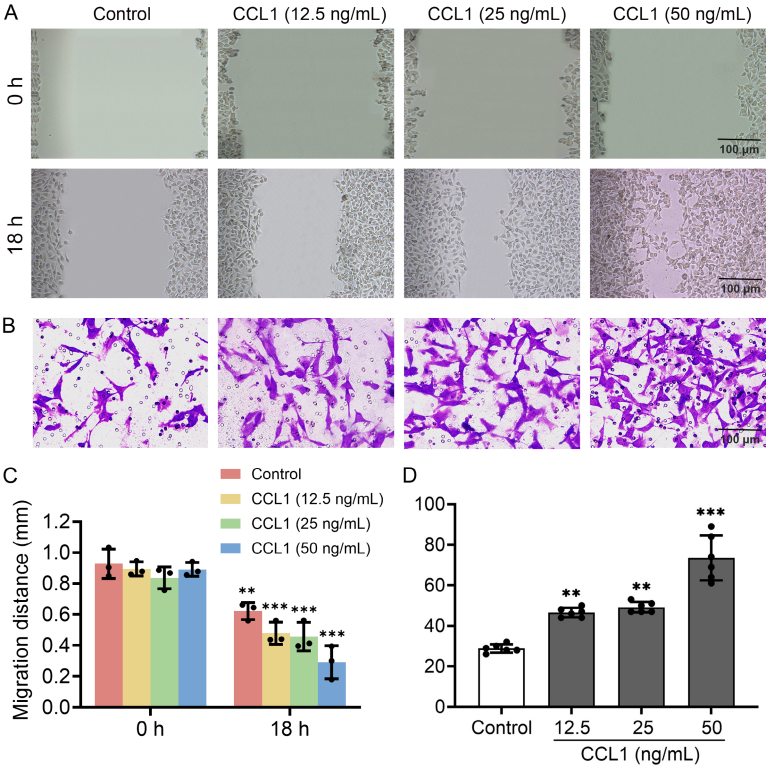

Figure 4. Effect of CCL1 on B16F10 cell migration and invasion. B16F10 cells were treated with CCL1, and migration and invasion assays were performed. (A) Representative images of migratory B16F10 cells. (B) Representative images of invasive B16F10 cells. (C) CCL1 significantly increased B16F10 cell migration in a concentration-dependent manner. (D) CCL1 significantly increased B16F10 cell invasion in a concentration-dependent manner. Scale bars, 100 μm (magnification: 200×) in (A, B). Data are presented as the means ± SD. *$P < 0.05$; **$P < 0.01$; ***$P < 0.001$.

CCL1 promotes the migration and invasion of B16F10 cells

To determine whether CCL1 affects the migration and invasion of B16F10 cells in vitro, wound-healing and Matrigel invasion assays were performed. Compared with PBS-treated control cells, CCL1-stimulated cells exhibited significantly increased migratory capacity (**Figure 4A**, **4C**). Treatment with various concentrations of CCL1 significantly increased the number of invading cells (**Figure 4B**, **4D**). These results show that CCL1 promotes B16F10 cell migration and invasion.

To further validate the functional role of CCL1 in B16F10 melanoma cell metastasis, we conducted blocking assays using R243, a specific inhibitor of CCL1. As shown in Figure S3, compared with treatment with CCL1 alone, cotreatment with R243 significantly decreased the migratory capacity of B16F10 cells and led to a marked reduction in the number of invading cells. These findings demonstrate that CCL1 is a critical downstream molecule responsible for the SAP-mediated suppression of melanoma migration and invasion.

CCL1 activates the Ras/MAPK pathway in melanoma

Previous studies have demonstrated that CCL1 can activate the Ras/MAPK pathway in BW5147 cells [26]. There-

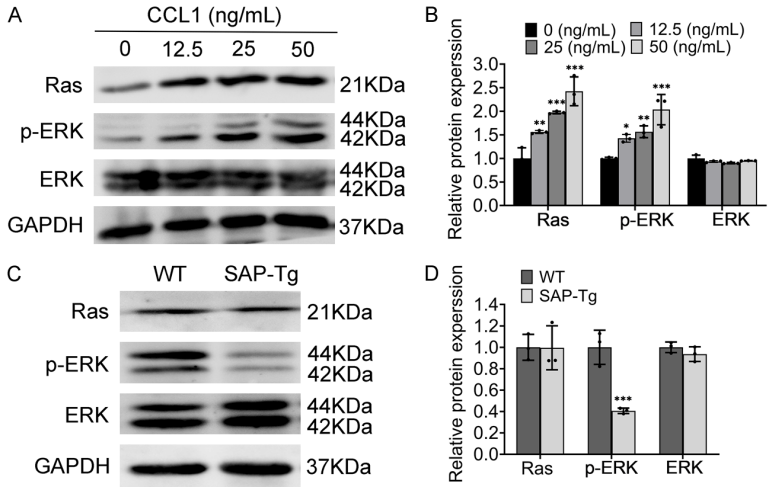

Figure 5. Effect of CCL1 on the Ras/MAPK pathway. A. Western blotting of B16F10 cells treated with different concentrations of CCL1 was performed. B. The statistical analysis showed that CCL1 promoted Ras and p-ERK expression but not ERK expression in B16F10 cells in a concentration-dependent manner. C. Western blotting of the homogenates of transplanted melanoma from WT and SAP-Tg mice was performed. D. The statistical analysis revealed that p-ERK expression was lower in SAP-Tg mice than in WT mice and that the levels of Ras and ERK were not different between WT and SAP-Tg mice. Data are presented as the means ± SD. **P < 0.05; **P < 0.01; ***P < 0.001.*

fore, we evaluated the effect of CCL1 on the Ras/MAPK pathway in B16F10 cells. As shown in **Figure 5A** and **5B**, CCL1 treatment upregulated the expression of Ras and phospho-ERK in a concentration-dependent manner. Phospho-ERK levels in the homogenates of SAP-Tg mice with transplanted melanoma cells were also decreased (**Figure 5C**, **5D**), whereas Ras expression did not significantly differ between the tumor homogenates of SAP-Tg and WT mice.

Discussion

In this study, we report that SAP significantly inhibits melanoma growth and metastasis by downregulating CCL1 expression, as determined using xenograft and metastasis mouse models developed with B16F10 melanoma cells. Specifically, SAP attenuated the secretion of CCL1 by mouse macrophages, which inhibited B16 cell migration and invasion. Furthermore, the SAP-induced downregulation of CCL1 expression inhibited the activation of the MAPK pathway.

SAP, a member of the short pentraxin family, plays a critical role in hepatic fibrosis, atherosclerosis, allergic airway disease and so forth. The serum concentration of SAP in patients with breast cancer and small cell lung cancer is correlated with breast cancer and small cell lung cancer [27, 28]. However, the effects of SAP on melanoma have not been reported. We used SAP-Tg mice to establish a mouse model of subcutaneously transplanted melanoma and found that SAP significantly inhibited melanoma growth. To further explore the effect of SAP on melanoma metastasis, melanoma lung metastasis and liver metastasis models were established in SAP-Tg and WT mice. SAP significantly inhibited both the lung metastasis and liver metastasis of melanoma. Malignant melanoma, which is among the most common skin cancers and one of the most aggressive cancers caused by melanocytes of the skin and other organs, is characterized by low incidence, high malignancy, early metastasis and high mortality [17]. Besides early surgical resection, specific treatments for malignant melanoma are lacking, and this disease has a poor prognosis [29]. Therefore, early diagnosis and timely and reasonable treatment of malignant melanoma are extremely important. Effective drugs for the treatment of malignant melanoma are currently lacking. The findings of this study provide additional favorable evidence of the clinical application of the SAP protein in the treatment of malignant melanoma. To this end, our findings have shown the promise of SAP as a novel therapeutic drug that may benefit cancer patients with malignant melanoma.

To explore how SAP suppresses melanoma growth and metastasis, we performed protein CHiP assays with the serum of WT and SAP-Tg mice transplanted with melanoma cells to identify genes that are known to be associated with inflammatory factors. We found that the serum concentration of CCL1 in SAP-Tg mice was significantly lower than that in WT mice. Our ELISA results also revealed that the concentration of CCL1 in the serum and tissue homogenates

was lower in tumor-bearing SAP-Tg mice than in tumor-bearing WT mice. These findings indicate that SAP decreases the level of CCL1, which inhibits melanoma growth and metastasis. CCL1 promotes M2-type macrophage T helper cell polarization in tumor tissues, thereby establishing the immune cell microenvironment and suppressing tumor progression [30]. Therefore, CCL1 secreted by tumor-infiltrating macrophages can promote tumor progression [31]. We also revealed that SAP inhibited the secretion of CCL1 by macrophages, but the mechanism by which SAP modulates macrophages to secrete CCL1 remains unclear. We also revealed that CCL1 promotes melanoma cell migration and invasion.

The results of the tumor xenograft and ELISA experiments suggested that CCL1 is involved in the inhibition of melanoma growth and metastasis. CCL1 can upregulate ERK1/2 MAPK phosphorylation in lymphoma cells. We observed that CCL1 upregulated Ras and p-ERK in B16F10 cells in a dose-dependent manner. Similarly, the levels of the Ras and p-ERK proteins were dramatically decreased in the tumor tissues of SAP-Tg mice. These findings indicate that SAP downregulates macrophage-secreted CCL1 to inhibit the Ras/p-ERK pathway. Although the role of the SAP-CCL1-Ras/MAPK axis has been clarified, the upstream regulatory mechanisms of CCL1 secretion and the direct effects of SAP on melanoma cells remain unclear. Moreover, potential regulatory pathways beyond the CCL1-Ras/MAPK cascade have not been fully investigated. Further coculture and receptor blockade experiments are needed to identify precise the molecular targets of SAP. The incidence of melanoma continues to increase among both males and females, particularly among individuals over 65 years of age [32]. Surgical resection and chemotherapy are the main treatments for malignant melanoma [33, 34], and at present, there are no effective drugs for the treatment of melanoma. SAP may be developed as a promising anti-malignant melanoma agent for clinical use.

Conclusion

Taken together, the results of this study demonstrated that SAP suppressed the growth and metastasis of malignant melanoma in melanoma xenograft and lung metastatic mouse models. The suppressive effect of SAP was achieved mainly through the suppression of CCL1 secretion by macrophages. Further study revealed that CCL1 promoted the migration and invasion of melanoma cells and activated the Ras/p-ERK pathway. While more research efforts are needed to determine the exact molecular mechanisms associated with the inhibitory effect of SAP on melanoma progression, SAP has shown great potential for melanoma treatment.

Acknowledgements

This study was supported by the National Natural Science Foundation of China (grant No.: 82302827), the Basic and Applied Basic Research Project of Guangdong Province (grant No.: 2026A1515012700), the Guangzhou Science and Technology Plan Project (grant No.: 2025A04J5306), the Project of Administration of Traditional Chinese Medicine of Guangdong Province (grant Nos.: 20242048 and 20251209), the Key Team of Basic and Clinical Research on Tumor Immunotherapy of Guangdong Pharmaceutical University (grant No.: 2024ZZ10), the Medical Scientific Research Foundation of Guangdong Province (grant No.: A2026094), and the Undergraduate Innovation Training Program Project (grant No.: S202510573003, S202610573022 and S202610573017).

Disclosure of conflict of interest

None.

Abbreviations

SAP, Serum amyloid P component; PTX, Pentraxin; CRP, C-reactive protein; CCL1, CC-chemokine 1; SAP-Tg mice, SAP-overexpressing mice; B16F10, Mouse melanoma cell line B16F10; PBS, Phosphate-buffered saline; H&E, Hematoxylin-eosin; BrdU, 5-Bromo-2'-deoxyuridine; DAB, Dimethylaminoazobenzene.

Address correspondence to: Lijing Wang and Cuiling Qi, Laboratory of Oncology and Immunology, School of Basic Medical Sciences, Guangdong Pharmaceutical University, No. 280 Waihuan East Road, Higher Education Mega Centre, Guangzhou 510006, Guangdong, China. E-mail: wanglijing62@163.com (LJW); qicuiling@gdpu.edu.cn (CLQ)

References

[1] Yang R, Hu J, Zeng B, Yang D, Li D, Yang M, Fan X, Li X, Mao X, Liu Y, Lyu Y and Li Y. Structural characterization of immune receptor family short pentraxins, C-reactive protein and serum amyloid P component, in primates. Dev Comp Immunol 2022; 130: 104371.

[2] Wang Z, Wang X, Zou H, Dai Z, Feng S, Zhang M, Xiao G, Liu Z and Cheng Q. The basic characteristics of the pentraxin family and their functions in tumor progression. Front Immunol 2020; 11: 1757.

[3] Levo Y, Wollner S and Treves AJ. Serum amyloid P-component levels in patients with malignancy. Scand J Immunol 1986; 24: 147-151.

[4] Merchant S and Korbelik M. Upregulation of genes for C-reactive protein and related pentraxin/complement proteins in photodynamic therapy-treated human tumor cells: enrolment of PI3K/Akt and AP-1. Immunobiology 2013; 218: 869-874.

[5] Cong M, Carvalho Gontijo Weber R, Sakane S, Zhang V, Jiang C, Taura K, Kodama Y, DeMinicis S, Ganguly S, Brafman D, Chien S, Kramer M, Lupher M, Brenner DA, Xu J and Kisseleva T. Serum amyloid P (PTX2) attenuates hepatic fibrosis in mice by inhibiting the activation of fibrocytes and HSCs. Hepatol Commun 2024; 8: e0557.

[6] Chacko L, Boldrini M, Martone R, Law S, Martinez-Naharrro A, Hutt DF, Kotecha T, Patel RK, Razvi Y, Rezk T, Cohen OC, Brown JT, Srikantharajah M, Ganesananthan S, Lane T, Lachmann HJ, Wechalekar AD, Sachchithanantham S, Mahmood S, Whelan CJ, Knight DS, Moon JC, Kellman P, Gillmore JD, Hawkins PN and Fontana M. Cardiac magnetic resonance-derived extracellular volume mapping for the quantification of hepatic and splenic amyloid. Circ Cardiovasc Imaging 2021; 14: e012506.

[7] Castiglione V, Franzini M, Aimo A, Carecci A, Lombardi CM, Passino C, Rapezzi C, Emdin M and Vergaro G. Use of biomarkers to diagnose and manage cardiac amyloidosis. Eur J Heart Fail 2021; 23: 217-230.

[8] Wechalekar A, Antoni G, Al Azzam W, Bergström M, Biswas S, Chen C, Cheriyan J, Cleveland M, Cookson L, Galette P, Janiczek RL, Kwong RY, Lukas MA, Millns H, Richards D, Schneider I, Solomon SD, Sörensen J, Storey J, Thompson D, van Dongen G, Vugts DJ, Wall A, Wikström G and Falk RH. Pharmacodynamic evaluation and safety assessment of treatment with antibodies to serum amyloid P component in patients with cardiac amyloidosis: an open-label Phase 2 study and an adjunctive immuno-PET imaging study. BMC Cardiovasc Disord 2022; 22: 49.

[9] Pilling D and Gomer RH. The development of serum amyloid P as a possible therapeutic. Front Immunol 2018; 9: 2328.

[10] Moreira AP, Cavassani KA, Hullinger R, Rosada RS, Fong DJ, Murray L, Hesson DP and Hogaboam CM. Serum amyloid P attenuates M2 macrophage activation and protects against fungal spore-induced allergic airway disease. J Allergy Clin Immunol 2010; 126: 712-721, e7.

[11] Murray LA, Kramer MS, Hesson DP, Watkins BA, Fey EG, Argentieri RL, Shaheen F, Knight DA and Sonis ST. Serum amyloid P ameliorates radiation-induced oral mucositis and fibrosis. Fibrogenesis Tissue Repair 2010; 3: 11.

[12] Wang H, Nie Y, Sun Z, He Y and Yang J. Serum amyloid P component: structure, biological activity, and application in diagnosis and treatment of immune-associated diseases. Mol Immunol 2024; 172: 1-8.

[13] Castaño AP, Lin SL, Surowy T, Nowlin BT, Turlapati SA, Patel T, Singh A, Li S, Lupher ML Jr and Duffield JS. Serum amyloid P inhibits fibrosis through Fc gamma R-dependent monocyte-macrophage regulation in vivo. Sci Transl Med 2009; 1: 5ra13.

[14] Chen W, Karhadkar TR, Ryu C, Herzog EL and Gomer RH. Reduced sialylation and bioactivity of the antifibrotic protein serum amyloid P in the sera of patients with idiopathic pulmonary fibrosis. Immunohorizons 2020; 4: 352-362.

[15] Yan J, Liu D, Wang J, You W, Yang W, Yan S and He W. Rewiring chaperone-mediated autophagy in cancer by a prion-like chemical inducer of proximity to counteract adaptive immune resistance. Drug Resist Updat 2024; 73: 101037.

[16] Atkins MB, Curiel-Lewandrowski C, Fisher DE, Swetter SM, Tsao H, Aguirre-Ghiso JA, Soengas MS, Weeraratna AT, Flaherty KT, Herlyn M, Sosman JA, Tawbi HA, Pavlick AC, Cassidy PB, Chandra S, Chapman PB, Daud A, Eroglu Z, Ferris LK, Fox BA, Gershenwald JE, Gibney GT, Grossman D, Hanks BA, Hanniford D, Hernando E, Jeter JM, Johnson DB, Khleif SN, Kirkwood JM, Leachman SA, Mays D, Nelson KC, Sondak VK, Sullivan RJ and Merlino G; Melanoma Research Foundation. The state of melanoma: emergent challenges and opportunities. Clin Cancer Res 2021; 27: 2678-2697.

[17] Xu M, Kong L and Jamil M. Advancements in skin cancer treatment: focus on photodynamic therapy: a review. Am J Cancer Res 2024; 14: 5011-5044.

[18] Rey-Barroso L, Peña-Gutiérrez S, Yáñez C, Burgos-Fernández FJ, Vilaseca M and Royo S. Optical technologies for the improvement of skin cancer diagnosis: a review. Sensors (Basel) 2021; 21: 252.

[19] Zhang H, Zhang Z, Jiang M, Wang S, Wang J, Wang H, Liu Y, Wang Y, Fu J, Wang P, Miao M,

Kim MO and Fang X. Triptolide suppresses melanoma cell growth *in vitro* and *in vivo* through the Src-ERK signaling pathway. J Cancer 2024; 15: 6345-6354.
[20] Teixido C, Castillo P, Martinez-Vila C, Arance A and Alos L. Molecular markers and targets in melanoma. Cells 2021; 10: 2320.
[21] Barrio-Alonso C, Nieto-Valle A, García-Martínez E, Gutiérrez-Seijo A, Parra-Blanco V, Márquez-Rodas I, Avilés-Izquierdo JA, Sánchez-Mateos P and Samaniego R. Chemokine profiling of melanoma-macrophage crosstalk identifies CCL8 and CCL15 as prognostic factors in cutaneous melanoma. J Pathol 2024; 262: 495-504.
[22] Villani A, Potestio L, Fabbrocini G, Troncone G, Malapelle U and Scalvenzi M. The treatment of advanced melanoma: therapeutic update. Int J Mol Sci 2022; 23: 6388.
[23] Basson C, Serem JC, Bipath P and Hlophe YN. Chemokines as possible therapeutic targets in metastatic melanoma. Cancer Med 2023; 12: 14387-14402.
[24] Kato T, Matsuo Y, Ueda G, Murase H, Aoyama Y, Omi K, Hayashi Y, Imafuji H, Saito K, Morimoto M, Ogawa R, Takahashi H and Takiguchi S. Enhanced CXCL12/CXCR4 signaling increases tumor progression in radiation-resistant pancreatic cancer. Oncol Rep 2022; 47: 68.
[25] Zhao HQ and Jiang J. Chemokines and receptors in the development and progression of malignant tumors. Cytokine 2023; 170: 156335.
[26] Louahed J, Struyf S, Demoulin JB, Parmentier M, Van Snick J, Van Damme J and Renauld JC. CCR8-dependent activation of the RAS/MAPK pathway mediates anti-apoptotic activity of I-309/CCL1 and vMIP-I. Eur J Immunol 2003; 33: 494-501.
[27] Xie H, Ruan G, Wei L, Zhang H, Shi J, Lin S, Liu C, Liu X, Zheng X, Chen Y, Deng L and Shi H. Obesity-associated metabolic inflammation promotes triple-negative breast cancer progression through the interleukin-6/STAT3/pentraxin 3/matrix metalloproteinase 7 axis. Int Immunopharmacol 2024; 136: 112332.
[28] Zhao J, Chi A, Mao R, Hu G and Ji M. Serum amyloid P-component level may be a biomarker for lung toxicities and overall survival after thoracic radiotherapy for non-small cell lung cancer. Clin Lab 2016; 62: 2183-2190.
[29] Huang K and Kim MO. Therapeutic strategies for drug-resistant melanoma and their clinical implications. J Cancer Prev 2025; 30: 7-11.
[30] Fujikawa M, Koma YI, Hosono M, Urakawa N, Tanigawa K, Shimizu M, Kodama T, Sakamoto H, Nishio M, Shigeoka M, Kakeji Y and Yokozaki H. Chemokine (C-C Motif) ligand 1 derived from tumor-associated macrophages contributes to esophageal squamous cell carcinoma progression via CCR8-mediated Akt/proline-rich akt substrate of 40 kDa/mammalian target of rapamycin pathway. Am J Pathol 2021; 191: 686-703.
[31] Hou PP, Luo LJ, Chen HZ, Chen QT, Bian XL, Wu SF, Zhou JX, Zhao WX, Liu JM, Wang XM, Zhang ZY, Yao LM, Chen Q, Zhou D and Wu Q. Ectosomal PKM2 promotes HCC by inducing macrophage differentiation and remodeling the tumor microenvironment. Mol Cell 2020; 78: 1192-1206, e10.
[32] Joshi UM, Kashani-Sabet M and Kirkwood JM. Cutaneous melanoma: a review. JAMA 2025; 334: 2113-2125.
[33] Long GV, Swetter SM, Menzies AM, Gershenwald JE and Scolyer RA. Cutaneous melanoma. Lancet 2023; 402: 485-502.
[34] Wagle NS, Nogueira L, Devasia TP, Mariotto AB, Yabroff KR, Islami F, Jemal A, Alteri R, Ganz PA and Siegel RL. Cancer treatment and survivorship statistics, 2025. CA Cancer J Clin 2025; 75: 308-340.

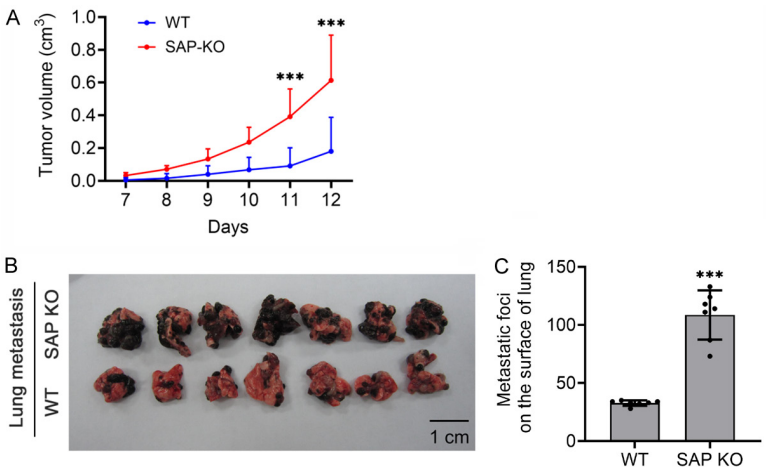

Figure S1. SAP deficiency promotes lung metastasis and primary tumor growth of B16F10 cells. A. The length and width of tumors from subcutaneously injected B16F10 cells were measured, and their volume was calculated. The average tumor volume of each mouse group was plotted against time. B. Gross images of melanoma lung metastasis in WT and SAP KO mice. C. Quantitative analysis of metastatic foci on the lung surface. Scale bars, 1 cm in (B). Data are presented as the means ± SD. ****P < 0.001*.

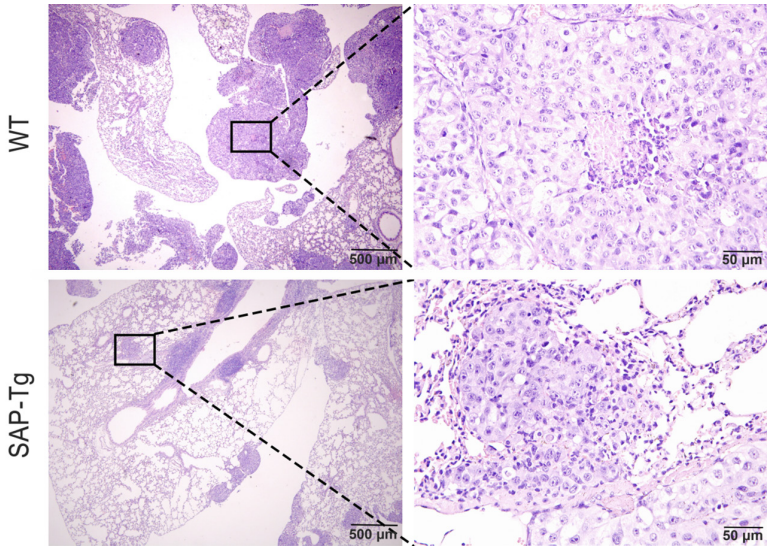

Figure S2. Representative H&E-stained sections of lung metastases from WT and SAP-Tg mice. The right panel shows a higher magnification of the black dotted squares in left panel. Scale bars: 500 μm (magnification: 40×); 50 μm (magnification: 400×).

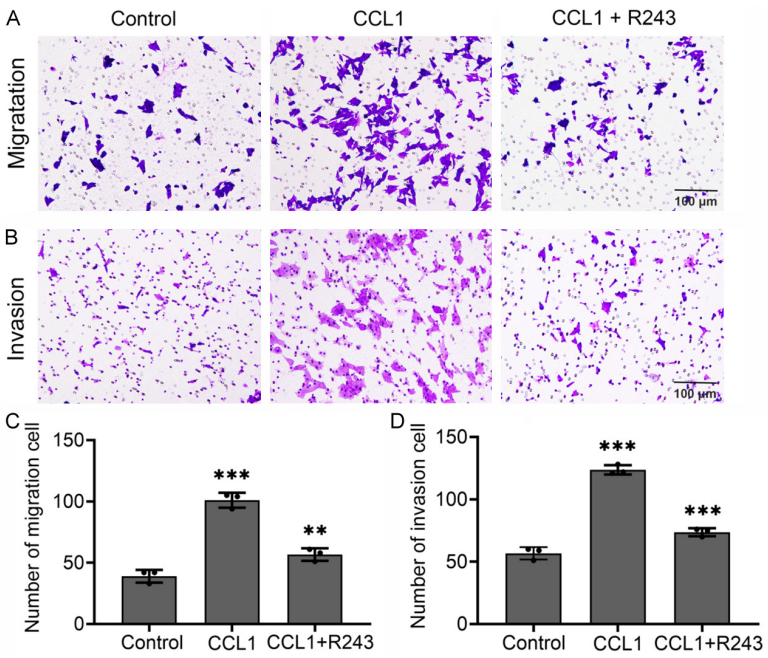

Figure S3. R243 reverses CCL1-induced migration and invasion in B16F10 cells. B16F10 cells were treated with CCL1, CCL1+ R243, and then subjected to migration and invasion assays. A. Representative images of migratory B16F10 cells. B. Representative images of invasive B16F10 cells. C. Quantification of migratory cell numbers. D. Quantification of invasive cell numbers. Scale bars: 100 μm, magnification: 200×. Data are presented as the means ± SD. ***P < 0.01; ***P < 0.001.*